International Space Planes and Hypersonic Systems and Technologies Conferences
6-9 July 2015, Glasgow, Scotland
20th AIAA International Space Planes and Hypersonic Systems and Technologies Conference

Experimental and Numerical Performance Analysis of a Self Starting, Three-Dimensional SCRamjet Intake

Andreas K. Flock*, Ali Gülhan†
German Aerospace Center (DLR), 51147 Cologne, Germany

In the present paper, a three-dimensional intake model is investigated in a blow-down wind tunnel and results are compared and complemented with numerical simulations (Reynolds-averaged Navier-Stokes simulations). The intake model was equipped with a movable cowl and therefore the internal contraction ratio was variable and was adjusted to the self starting condition. Three different conditions were investigated: i) at a free stream Mach number of 7, a v-shaped cowl geometry was investigated, ii) at a free stream Mach number of 7 a straight cowl geometry was investigated, and iii) the v-shaped cowl geometry was investigated at a free stream Mach number of 6. Furthermore a one-dimensional post analysis was performed, to calculate overall engine parameter from stream thrust averaged intake performance parameter. The numerical simulations were validated on the basis of wall pressure and rake pressure measurements and the match was generally well. Performance wise, the v-shaped cowl was slightly superior compared to the straight cowl. For the Mach 7 configurations maximum back pressure ratios of approximately 120 were measured, which is about 4 times the nominal operating pressure ratio. For the Mach 6 case, the maximum static back pressure ratio dropped to about 80, which again is approximately 4 times the nominal operating pressure ratio.

Nomenclature

A	area, $[\mathrm{m}^2]$	s-lip	straight lip geometry
CAD	computer aided design	str-thr-av	stream thrust averaged
CFD	computational fluid dynamics	T	temperature, $[\mathrm{K}]$
CR	contraction ratio	v-lip	v-lip geometry
D	diameter, $[\mathrm{m}]$	x, y, z	spatial coordinates, $[\mathrm{m}]$
EXP	experimental/experiment	$y+$	non dimensional wall distance
F	force, $[\mathrm{N}]$	α/β	pitch/yaw angle
I	impulse, $[\mathrm{s}]$	γ	ratio of specific heats
LHV	lower heating value	η	efficiency
m	mass-ratio	Θ	temperature ratio
m-av	mass averaged	Π	pressure ratio
M	Mach number	φ	equivalence ratio
p	pressure, $[\mathrm{N/m}^2]$		
Re	Reynolds number		

Subscript

cl	cowl closure	st	static
H	hydraulic	stoi	stoichiometric
i	internal portion	t	total
o	overall portion	th	throat
sp	specific	∞	free stream condition

I. Introduction

Hypersonic flight within the earth's atmosphere offers advantages for military as well as civil applications. Air breathing engines usually have better efficiency than rocket engines, because air from the surrounding atmosphere is used as their oxidizer. One air breathing engine cycle, suitable for hypersonic flight, is the supersonic combustion

*PhD Candidate, Supersonic and Hypersonic Technology Department, Institute of Aerodynamics and Flow Technology, Linder Höhe, 51147 Cologne, Germany, AIAA Student Member
†Department Head, Supersonic and Hypersonic Technology Department, Institute of Aerodynamics and Flow Technology, Linder Höhe, 51147 Cologne, Germany

ramjet (SCRamjet). In a SCRamjet engine, air is compressed in the intake, and passes through a short isolator section into the combustion chamber. In the combustion chamber, fuel is injected, mixed and burned, and finally exhausted through a nozzle.

In the present paper, we will focus on the intake, which compresses the air flow to conditions suitable for supersonic combustion. For hydrogen combustion, a static pressure and temperature of $50,000\ \mathrm{Pa}$ and $1000\ \mathrm{K}$ are regarded as sufficient, while the static pressure mainly influences the combustion length, and the static temperature determines the ignition delay[1] chap. 4. Various parameter exist, which describe the intake performance and an overview is given in[2,3]. Static pressure and temperature ratios are defined as

$$\Pi_{\mathrm{st}} = \frac{p_{\mathrm{cc}}}{p_{\infty}} \tag{1}$$

and

$$\Theta_{\mathrm{st}} = \frac{T_{\mathrm{cc}}}{T_{\infty}}, \tag{2}$$

while the subscript cc denotes the position at the intake exit, or the combustion chamber entrance. Furthermore, total pressure as well as total temperature ratios are defined as

$$\Pi_{\mathrm{t}} = \frac{p_{\mathrm{t,cc}}}{p_{\mathrm{t},\infty}} \tag{3}$$

and

$$\Theta_{\mathrm{t}} = \frac{T_{\mathrm{t,cc}}}{T_{\mathrm{t},\infty}}. \tag{4}$$

The total temperature ratio in the intake is influenced by the wall boundary condition. For moderate wall temperatures ($T_{\mathrm{t},\infty}/T_{\mathrm{w}} \approx 2$), the loss in total temperature is relatively low ($\approx 5\%$). The total pressure ratio, which is sometimes referred to as total pressure recovery, is a measure for the efficiency of the compression, while $\Pi_{\mathrm{t}} = 1$ corresponds to isentropic compression. The kinetic energy efficiency is the ratio of kinetic energy that the intake exit flow would have, if it would be expanded isentropically to free stream pressure, divided by the kinetic energy of the free stream, and together with the free stream Mach number can be directly related to the total pressure recovery:

$$\eta_{\mathrm{KE}} = 1 - \frac{2}{(\gamma-1)M_{\infty}^2}\left(\left(\frac{1}{\Pi_{\mathrm{t}}}\right)^{(\gamma-1)/\gamma} - 1\right) \tag{5}$$

Friction drag and shock losses reduce total pressure, and the goal of the intake designer is to minimize these losses. Smart[4] divided the performance parameters into *capability* parameters, which describe the amount of compression, and *efficiency* parameters, such as the total pressure recovery or kinetic energy efficiency. Usually with increasing pressure level, it becomes harder to design highly efficient intakes, and Smart noted, that capability as well as efficiency parameter should be included in a performance analysis.

The investigated intake configurations are all self starting configurations. The starting capability as well as a detailed discussion of intake starting in general is given in[5]. Intake performance parameter for a certain configuration can either be determined via analytical, experimental or numerical means. Because the intake of the present study was designed with a CFD parameter study, there are no analytical tools to predict its performance. Therefore in the present study we used wind tunnel experiments and numerical simulations subsidiary to determine the intake performance.

The focus of the present paper is, to quantify performance parameter of the three-dimensional intake. Thereto, we will discuss the experiments, performed in the H2K wind tunnel facility and compare the results with numerical simulations. The numerical simulations and wind tunnel experiments together will deliver a deeper insight into the intake performance, than one by itself. Finally we transferred the wind tunnel conditions to flight conditions, and performed numerical simulations. Together with a simple one-dimensional analysis, containing the combustion chamber and SCRamjet nozzle, the overall performance parameter specific impulse and specific thrust were calculated.

II. Methods and Materials

In the following we shortly describe the intake model, as well as the experimental and numerical setup. Furthermore the investigated conditions as well as the one-dimensional post processing techniques are presented.

A. SCRamjet Intake Model

The three-dimensional SCRamjet intake model was designed by means of a computational fluid dynamics (CFD) parameter study by Hohn[6] and Riehmer[7], and a CAD image is displayed in figure 1. The inclination angle of the main ramp was $8\ \mathrm{deg}$, and the side walls converged with $7\ \mathrm{deg}$ on each side. The sweep angle at the leading edge was $50\ \mathrm{deg}$

and continuously decreased along intake length. The overall contraction ratio, CR_{o}, of the intake was 8.12, while the internal contraction ratio, CR_{i}, could be varied between 1.28 and 2.56 due to a movable cowl. A $v-$shaped and straight version of the cowl were manufactured to investigate the influence of cowl geometry and overboard spillage on intake performance.

On the symmetry plane, along the bottom and top wall, static pressure sensors were installed, and pressures were recored with PSI modules (Pressure Systems Inc.), which sampled with ≈ 3Hz. Further pressure sensors were located in the intake cowl, and circumferentially at two axial positions. At the intake exit, a pitot rake was positioned, which was equipped with alternating pitot as well as static pressure probes[8]. Because the length of the pressure ducts was relatively short (≈ 0.5 m), the pressure response was faster than the relatively low sampling rate. The length from the leading edge to the position of the pitot rake was 722 mm, and the throat area was 40×65 mm^2 with rounded corners ($r = 10$ mm). The intake throat was located at 650 mm, and after that a diverging section was added. The top and bottom wall opened with 1 deg each, while the side walls remained constant. A schlieren system was installed[9], to record the shock structure at the frontal part of the intake, and the field of view is displayed in figure 1.

To the intake model, a settling chamber was attached, which was mounted to the wind tunnel fixture. At the end of the settling chamber a conical throttle was attached, and the inner conical part could be moved in stream wise direction. The throttle had two functions: First, an artificial back pressure could be imposed on the intake model, and the changes in performance could be investigated. Thereto, the inner part of the throttle was moved upstream and the smallest cross section at the throttle exit decreased. Consequently, the pressure increased within the settling chamber and at the intake exit. Second, following norm ISO 5167-1, the mass flow through the intake model could be measured. Together with static pressure and total temperature measurements within the settling chamber, and assuming that the flow within the settling chamber was subsonic and accelerated to $M = 1$ at the throttle throat, the mass flow through the intake model could be calculated. However, we note that for this procedure, the flow within the settling chamber needed to be subsonic, which was satisfied at higher throttling ratios only.

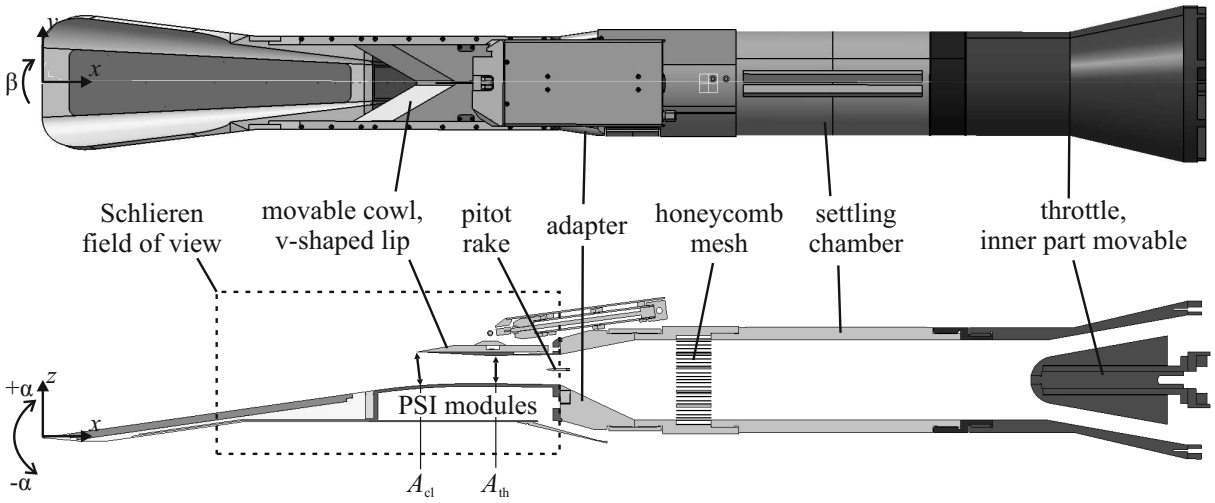

Figure 1: CAD image of top and cross sectional view of 3D SCRamjet intake with attached throttle.

Three intake configurations were investigated and are summarized in table 1. Two different cowl geometries were investigated, and for the v-shaped cowl, the influence of Mach number on the performance was investigated. Because we adjusted the intake configuration to the self starting condition, the internal contraction ratio varied, and for Mach 7 was at 1.92 and 2.12 for the v-lip and straight lip, respectively. For Mach 6 the internal contraction reduced to 1.73.

Table 1: Investigated intake configurations.

	M7v	M7s	M6v
M	7	7	6
lip configuration	v-lip	straight lip	v-lip
CR_{i}	1.92	2.12	1.73

B. Experimental Facility

The H2K wind tunnel, which was used for the experiments (figure 2), is a cold flow, blow down wind tunnel[10]. From a high pressure reservoir, air was led into electric heaters, which heated up the air stream to desired temperatures. During this heating process, air was released into the atmosphere. Once the temperatures were reached, a valve was triggered, and the air stream was released through a Laval nozzle into the test section, before exiting through a diffuser into the vacuum sphere. Depending on the desired conditions, testing times of up to 35 s could be achieved. There are five Laval nozzles, all with an exit diameter of 600 mm, for Mach 5.3, 6, 7, 8.7, and 11.2 conditions. The wind tunnel conditions which we used will be described in detail in a subsequent section.

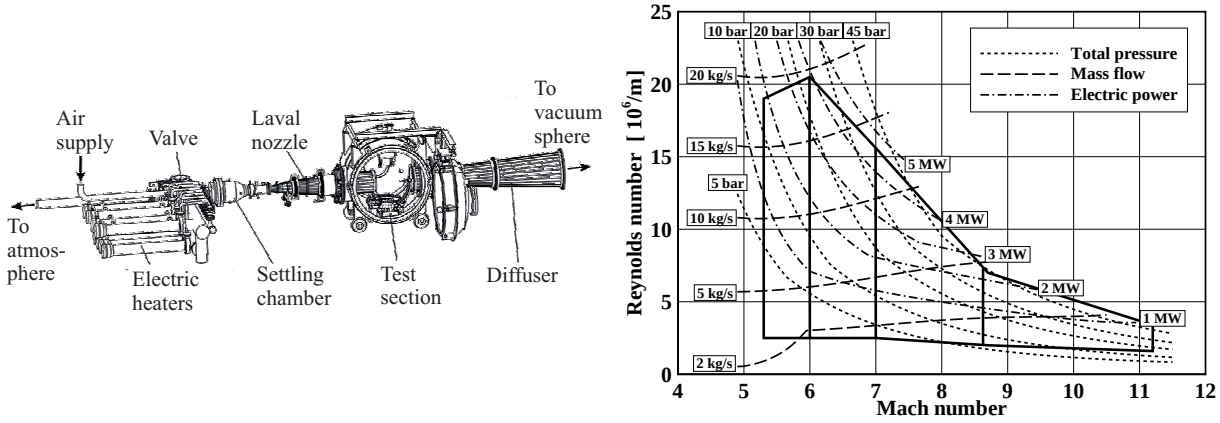

Figure 2: Schematic setup of the H2K wind-tunnel[10] (left) along with flow conditions diagram (right).

C. Numerical Modeling

Reynolds-averaged Navier-Stokes simulations were performed with the DLR finite volume solver TAU[11]. For the turbulence modeling, the Wilcox $k-\omega$ SST turbulence model was used[12]. An isothermal boundary condition was used at the intake wall and the inviscid fluxes were reconstructed with a second order upwind scheme.

For the mesh generation, the Centaur (v10.5) software package was used. Near viscous wall boundaries, structured elements were used, while unstructured elements were used for the remaining domain. A non dimensional wall distance of $y+ < 1$ was assured and approximately 35 layers were used. Grids consisted of approximately 0.1×10^6 and 0.8×10^6 grid points and elements, respectively. The adaptation tool, implemented in TAU, was used to refine the grids, and eventually the grids consisted of approximately 6×10^6 and 18×10^6 grid points and elements, respectively.

D. Wind Tunnel and Flight Conditions

During the wind tunnel experiments, the Reynolds number was set according to free flight conditions along a constant dynamic pressure trajectory $q_\infty = 0.53$ bar. The Mach 6 and Mach 7 nozzles were used, and during the experiments the total temperature was set to $T_\mathrm{t} = 700$ K, while the Reynolds number was adjusted via the reservoir total pressure. The model heated up during an experiment, but due to the massive structure the temperature increase of the model was relatively low and a constant wall temperature of $T_\mathrm{w} = 300$ K was used for the simulations.

For flight conditions, the total to wall temperature ratio was set to the same value, and therefore during the simulations the wall temperatures were 1000 K and 800 K for the Mach 7 and 6 case, respectively. The investigated wind tunnel and flight conditions are summarized in table 2.

Table 2: Wind tunnel and flight conditions.

	M	$p_{\mathrm{t},\infty}$ [bar]	$T_{\mathrm{t},\infty}$ [K]	Re [1/m]	$p_{\mathrm{st},\infty}$ [Pa]	$T_{\mathrm{st},\infty}$ [K]
H2K Condition	7 ± 0.05	10.4 ± 0.02	700 ± 20	3.39×10^6	251	65
	6 ± 0.05	8.3 ± 0.02	700 ± 20	4.01×10^6	523	85
Flight Condition	7	63.3	2430	3.39×10^6	1528	225
	6	32.8	1830	4.01×10^6	2080	223

E. One-Dimensional Post Analysis

To model the flow through the combustion chamber and nozzle we one-dimensionalized the flow field at the intake exit and further processed the flow in an analytical tool. The procedure will be described in the subsequent paragraphs:

1. Combustion Chamber

The combustion chamber was modeled by a sudden heat release to simulate the combustion, and a subsequent duct with area change and frictional flow to represent viscous forces within the SCRamjet. Hydrogen was used as fuel, and the lower heating value (LHV) was 119×10^6 J/kg. The changes in properties due to heat release were calculated with the Rayleigh-flow equations, which are valid for inviscid and steady flow and can be found in [13]. The general procedure is repeated in the following:

1. Calculate the change in total temperature/enthalpy due to the heat release of the fuel, with the respective equivalence ratio and combustion efficiency, which we set to $\eta_{\mathrm{cc}} = 0.8 = const.$:

$$h_{\mathrm{t},4} = h_{\mathrm{t},3} + \eta_{\mathrm{cc}} \mathrm{LHV} \frac{\varphi}{m_{\mathrm{stoi}}} \tag{6}$$

2. With the total temperature, a Mach number can be calculated via:

$$\frac{T_{\mathrm{t},4}}{T_{\mathrm{t},3}} = \frac{\left(1 + \frac{\gamma-1}{2} M_4^2\right) M_4^2}{\left(1 + \frac{\gamma-1}{2} M_3^2\right) M_3^2} \left(\frac{1+\gamma M_3^2}{1+\gamma M_4^2}\right)^2 \tag{7}$$

3. Finally, a temperature and pressure can be calculated via:

$$T_4 = T_{\mathrm{t},4} \left(1 + \frac{\gamma-1}{2} M_4^2\right)^{-1} \tag{8}$$

$$\frac{p_4}{p_3} = \frac{1+\gamma M_3^2}{1+\gamma M_4^2} \tag{9}$$

The changes in properties in the subsequent duct were calculated for steady, frictional and adiabatic flow. To calculate the Mach number in x-direction, the following differential equation was integrated numerically:

$$\frac{\mathrm{d}M}{M} = \underbrace{-\left(\frac{1+\frac{\gamma-1}{2}M^2}{1-M^2}\right)\frac{\mathrm{d}A}{A}}_{\text{influence of area change}} + \underbrace{\left(\frac{1+\frac{\gamma-1}{2}M^2}{1-M^2}\right)\frac{\gamma M^2}{2}\frac{4c_{\mathrm{f}}\mathrm{d}x}{D_{\mathrm{H}}}}_{\text{influence of friction}} \tag{10}$$

The friction-coefficient, c_{f}, was set to 0.02, and the length of the combustion chamber was 0.4 m. The opening angle of the combustor was 1 deg. With the Mach number distribution, the temperature and pressure could be calculated via:

$$\frac{\mathrm{d}T}{T} = -\frac{(\gamma-1)M^2}{1+\frac{(\gamma-1)}{2}M^2}\frac{\mathrm{d}M}{M} \tag{11}$$

$$\frac{\mathrm{d}p}{p} = -\frac{\mathrm{d}A}{A} + 0.5\frac{\mathrm{d}T}{T} - \frac{\mathrm{d}M}{M} \tag{12}$$

Further information on flow with friction and area change can be found in [14] chap. 9.

2. Nozzle

To model the flow through the nozzle, we used the isentropic flow relations for a given area ratio. Via equation:

$$\left(\frac{A_{10}}{A_4}\right)^2 = \left(\frac{M_4}{M_{10}}\right)^2 \left(\frac{1+\frac{\gamma-1}{2}M_{10}^2}{1+\frac{\gamma-1}{2}M_4^2}\right)^{\frac{\gamma+1}{\gamma-1}} \tag{13}$$

the change in Mach number for the given area ratio was calculated and with assuming inviscid and adiabatic flow, the pressure and temperature could be calculated.

$$p_4^{1-\gamma} T_4^{\gamma} = p_{10}^{1-\gamma} T_{10}^{\gamma} = const. \tag{14}$$

$$T_4 \left(1 + \frac{\gamma-1}{2} M_4^2\right) = T_{10} \left(1 + \frac{\gamma-1}{2} M_{10}^2\right) \tag{15}$$

The contraction ratio of the nozzle was set equal to the intake overall contraction ratio. Further information on isentropic flow through nozzles can be found in [15] chap. 10.

III. Results

In the present section, wall pressure measurements, the intake behavior under back pressure, rake measurements and the one-dimensional post analysis are presented.

A. Wall Pressure Plots

In figure 3, 4, and 5 normalized wall pressure plots are shown for numerical and experimental results of the three configurations. On the intake ramp, there is an excellent agreement between experiments and numerical values. Further downstream in the internal part of the intake, the wall pressure calculated with CFD slightly differs from the experimental results, which could be caused by not accurately capturing separation regions with the turbulence model. However, the overall changes are small.

The Mach 7 cases are quantitatively similar, except for the region underneath the intake cowl, where the pressure level is generally lower for the straight lip configuration. The general pressure level observed for the Mach 6 configuration is lower, caused by the lower Mach number and therefore generally weaker shock system.

Furthermore the mass averaged and stream thrust averaged static pressure ratios for $x > 0.55$ m, extracted from the numerical simulations, are plotted. For all cases, the averaged static pressure ratios increased until about $x = 0.65$ m, where the intake throat is located. In the diverging portion, the static pressure ratios dropped again. Furthermore it is noted, that the stream thrust averaged values were generally lower than the mass averaged values, which should be considered, when one-dimensional values are extracted and further used in analytical tools.

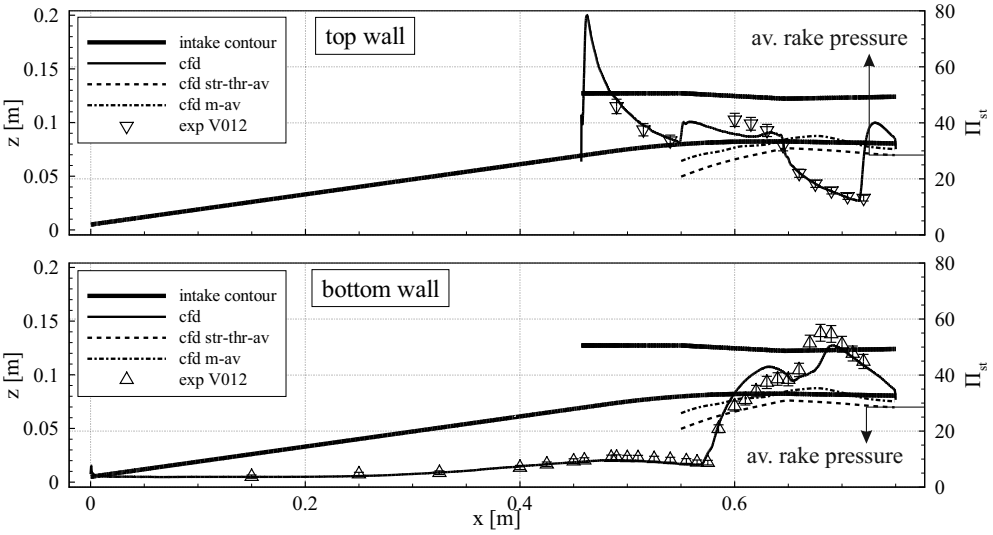

Figure 3: Comparison of experimental and numerical wall pressures, normalized to free stream pressure for $M_\infty = 7$, v-lip case; top - cowl wall, bottom - ramp wall; additionally stream thrust and mass averaged pressure distributions are shown.

B. Intake Behavior for Imposed Back Pressure

To simulate pressure peaks, which can occur in the combustor during the combustion process, a throttle was attached to the intake exit. For the three configurations, the throttle was closed and the pressure at the intake exit was measured with a rake located at $x = 0.722$ m. Normalized pressures are displayed in figure 6 and an increasing throttling ratio corresponded to a closing throttle and therefore higher blockage. Pressures were calculated by averaging the data of the static pressure probes at the intake rake.

For the Mach 7 cases the static pressure ratio in the non throttled case lied at around 30. When the intake was throttled, the pressure levels increased until ≈ 120 and then fluctuated around that level. Therefore the maximum static pressure ratio was approximately 4 times the operating static pressure ratio. When the Mach number was decreased to 6, the operating static pressure ratio dropped to 20. During throttling, the maximum back pressure was ≈ 80, and therefore lower than in the Mach 7 cases. However, the ratio of maximum static pressure to operating static pressure was constant.

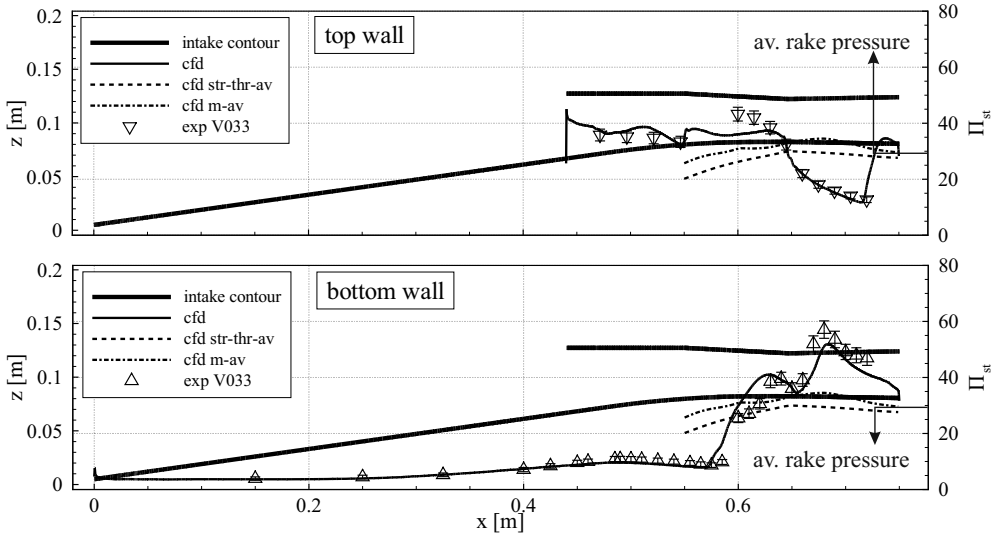

Figure 4: Comparison of experimental and numerical wall pressures, normalized to free stream pressure; top - cowl wall, bottom - ramp wall; additionally stream thrust and mass averaged pressure distributions are shown for $M_\infty = 7$, s-lip case.

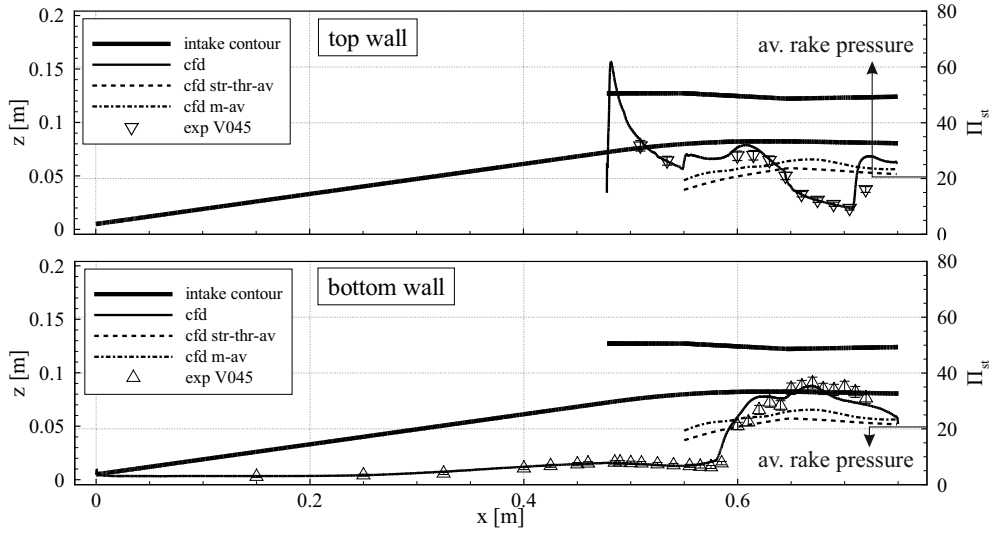

Figure 5: Comparison of experimental and numerical wall pressures, normalized to free stream pressure; top - cowl wall, bottom - ramp wall; additionally stream thrust and mass averaged pressure distributions are shown for $M_\infty = 6$, v-lip case.

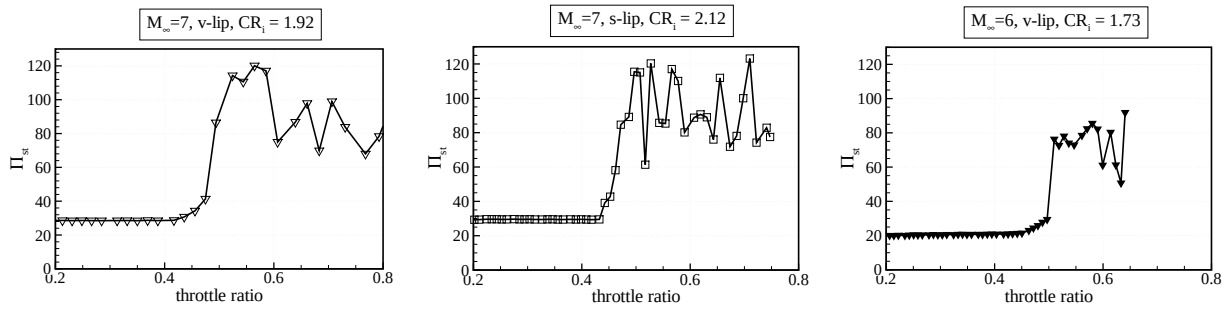

Figure 6: Intake exit pressure, measured at rake, plotted versus throttle ratio (throttle closes for increasing throttle ratio) for the three different self starting configurations.

C. Rake Measurements

In figures 7, 8, and 9 measurements along the horizontal and vertical part of the rake are plotted along with measurement uncertainties as error bars. Multiple measurements are plotted, to show fluctuations during a wind tunnel run. The diameter of a pressure tube was $0.7\,\mathrm{mm}$. Therefore CFD data is plotted for $z = 103 \pm 0.35\,\mathrm{mm}$ (horizontal ports) and $y = 0 \pm 0.35\,\mathrm{mm}$ (vertical ports) to illustrate the uncertainty in location. First, the static and pitot pressures are given, which were measured directly. From the static and pitot pressure, the Mach number was calculated, and is additionally plotted as a third variable.

Overall the data uncertainty of the in stream measurements is larger compared to the wall pressure measurements. This is caused by the generally larger uncertainty of the static and pitot tubes, but also by the fact, that pressures were partially interpolated from their neighboring values. Nevertheless the agreement between numerical data and experiments is generally good. In the subsequent context, the results will be discussed in more detail.

In the Mach 7 case the static pressure ratio decreased from $40 - 45$ at the bottom, to ≈ 15 at the top. In the numerical results a small high pressure region at the top was observed, which indicated an incoming sock wave. In horizontal direction, the static pressure measurements of the simulations behaved anti-cyclic to the experiments: While during the experiments the pressure in the middle and at the sides was higher and lower, respectively, during the simulations the opposite behavior was observed. The pitot pressure at the top was generally lower than at the bottom, while in the numerical simulations a plateau was detected at $z \approx 105\,\mathrm{mm}$, which was not present in the measurements. In horizontal direction, the measured and numerically calculated pitot pressures very nicely matched, with the only exception in the very center. There a static pressure port was located and the respective pitot pressure was interpolated from the neighboring values. The Mach numbers, which were calculated from the pitot and static pressure values were met very nicely in the vertical direction and only slightly differed at the sides.

Replacing the v-shaped lip with the straight lip had little influence on the numerical results. The experimental rake data was more affected by the change in cowl geometry. The pressure distributions of the straight lip configurations were less continuous, which indicated a more heterogeneous flow field.

In the Mach 6 case, pressures were generally lower, and numerical results matched the experiments better. The high pressure region at the top was detected to be larger by the numerical simulations, and in the experimental results a tendency towards an increase in pressure was visible.

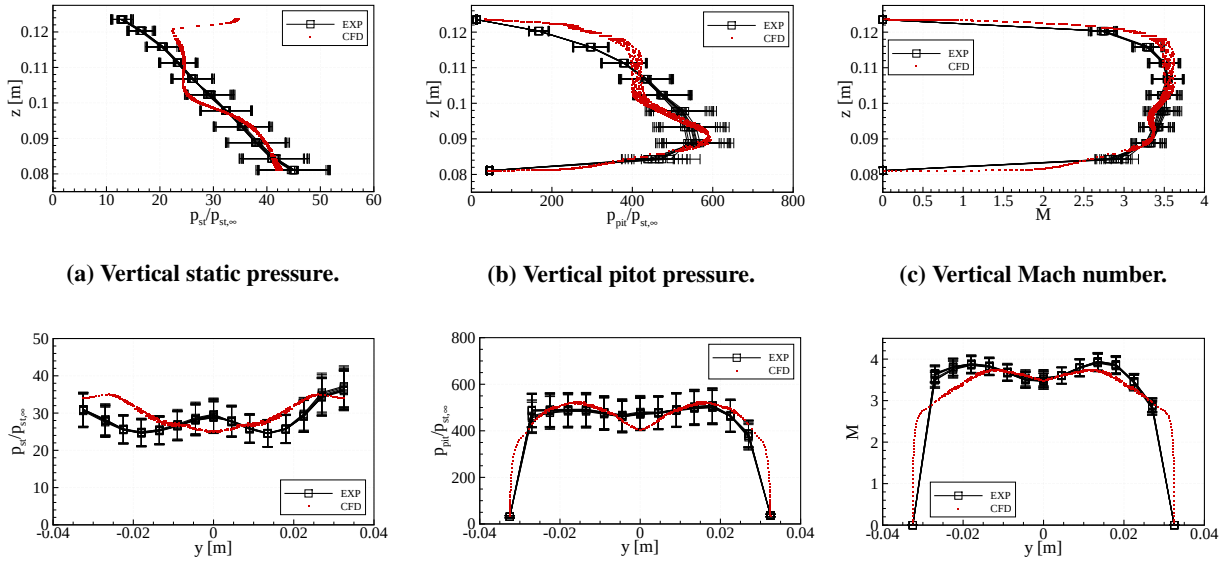

(a) Vertical static pressure. **(b) Vertical pitot pressure.** **(c) Vertical Mach number.**

(d) Horizontal static pressure. **(e) Horizontal pitot pressure.** **(f) Horizontal Mach number.**

Figure 7: Static and pitot pressure, as well as Mach number for the Mach 7, v-lip configuration, at $x = 0.722\,\mathrm{m}$.

In figure 10 we extracted contour plots from the numerical simulations to provide a better impression of the overall flow field. Data was extracted at $x = 722.3\,\mathrm{mm}$, and pressure was normalized with the respective free stream static condition.

In vertical direction, we observed a high pressure at the bottom and a low pressure at the top, which indicated a shock front of a shock train driving down the isolator. Along the horizontal axis, the pressure level is relatively constant, which matched the experimental results. Only a small shock front was visible at $y = 18 - 20\,\mathrm{mm}$. Furthermore the three-dimensionality of the flow was clearly visible.

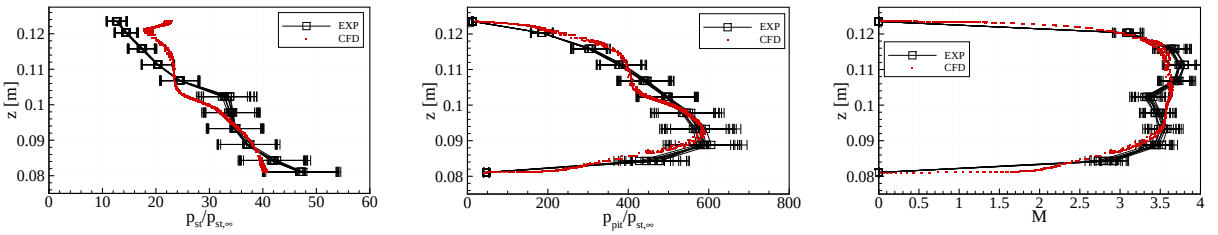

(a) Vertical static pressure. **(b) Vertical pitot pressure.** **(c) Vertical Mach number.**

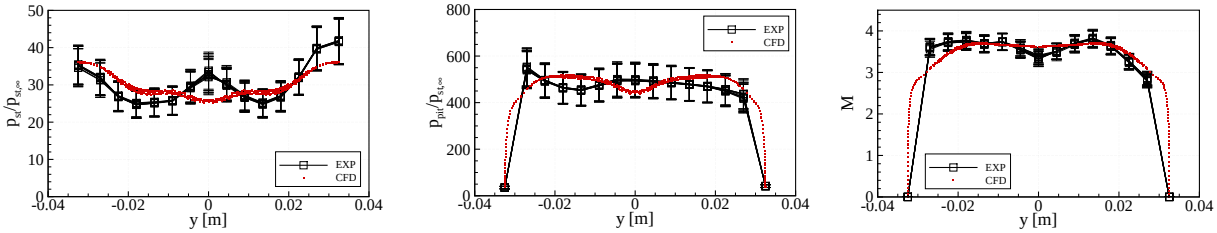

(d) Horizontal static pressure. **(e) Horizontal pitot pressure.** **(f) Horizontal Mach number.**

Figure 8: Static and pitot pressure, as well as Mach number for the Mach 7, s-lip configuration, at $x = 0.722$ m.

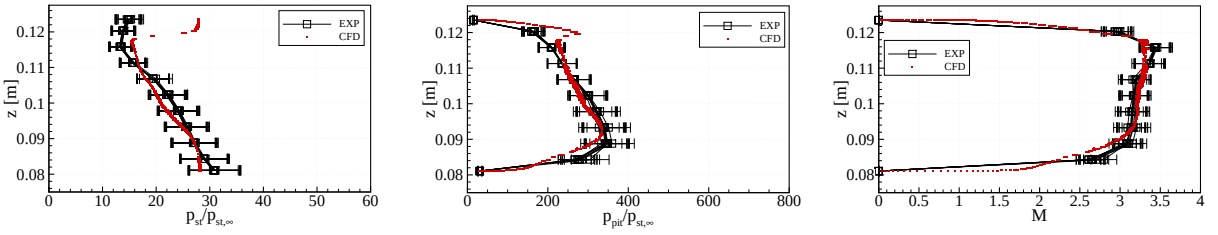

(a) Vertical static pressure. **(b) Vertical pitot pressure.** **(c) Vertical Mach number.**

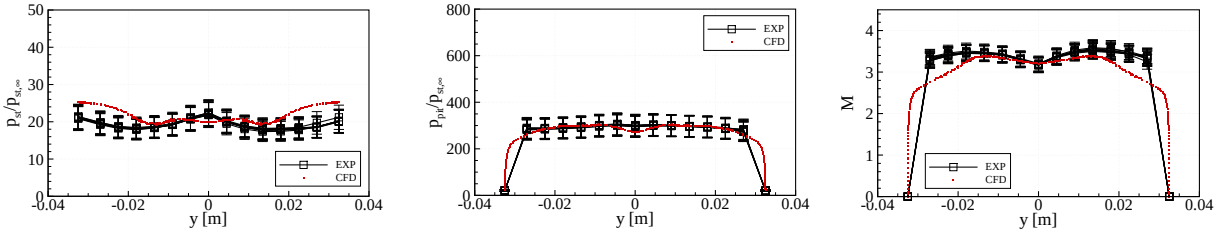

(d) Horizontal static pressure. **(e) Horizontal pitot pressure.** **(f) Horizontal Mach number.**

Figure 9: Static and pitot pressure, as well as Mach number for the Mach 6, v-lip configuration, at $x = 0.722$ m.

Because the rake spreads out along the horizontal and vertical axis of the cross section plane only, an averaged value would only reproduce a one dimensional quantity for this centered region, while the remaining parts of the top-left and -right, as well as the bottom-left and -right are neglected. This introduces an error to the one-dimensionalized variable, and it is a difficult question what method is more accurate: Averaging the entire CFD flow field, or obtaining an averaged value from the experimental results, which are available for discrete points only.

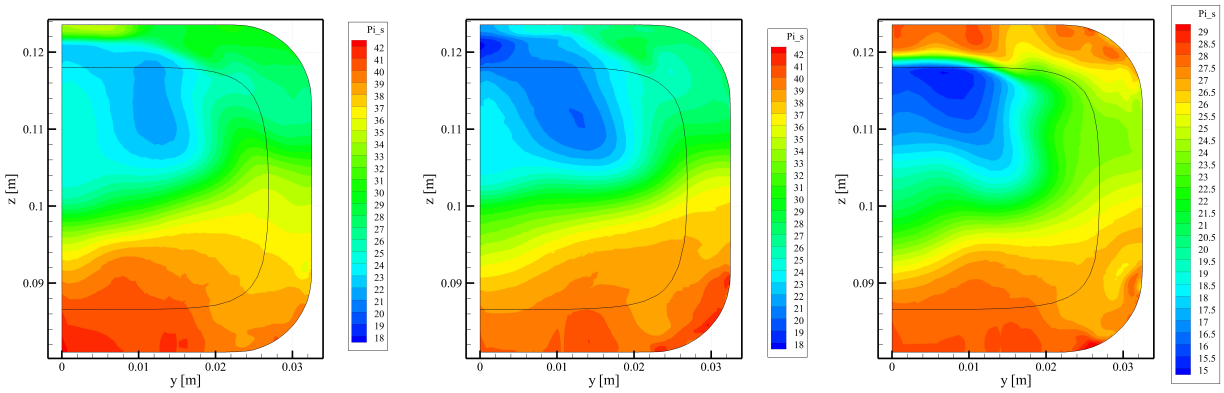

(a) Mach 7 and v-lip case. **(b) Mach 7 and s-lip case.** **(c) Mach 6 and v-lip case.**

Figure 10: Cross sectional planes, extracted from CFD at $x = 722.3$ mm.

D. One-Dimensional Post Analysis

To further process the SCRamjet data, we used the numerical simulations for flight conditions and extracted intake exit data. Flight conditions and exit conditions are summarized in table 2 and 3, respectively. Furthermore, intake performance parameters, calculated with the stream thrust averaged values are given and finally, we post-processed the data with the one-dimensional analysis described in section II. and calculated the overall engine parameters specific thrust, F_{sp}, specific impulse, I_{sp} and overall efficiency, η_{oa}.

First, the maximum equivalence ratio was calculated, which could be used without choking to occur in the combustion chamber and the level dropped from 0.47 for the Mach 7 configurations to 0.30 for the Mach 6 configuration. This relatively low level can be explained by not considering any heat losses into the combustor walls in the one-dimensional post analysis. The v-shaped lip slightly improved the engine performance for the Mach 7 configuration, and the maximum I_{sp} and F_{sp} for Mach 7 flight were around 2460 s and 330 N/(kg/s), respectively. For the Mach 6 configuration, the maximum I_{sp} and F_{sp} were ≈ 2940 s and ≈ 250 N/(kg/s), respectively.

Second, for a constant equivalence ratio of $\varphi = 0.30$, the engine performance was calculated for the three different configurations. Again, the v-shaped lip slightly improved the engine performance. However because of the less amount of fuel for the Mach 7 configurations the performance was lower. Finally we emphasize, that the values of the one-dimensional analysis only give a first estimate of the expected engine performance and more precise information would require more elaborate methods.

IV. Conclusion

In the current paper we presented numerical and experimental results of a three-dimensional SCRamjet intake, operating at its self starting conditions. The intake geometry and the experimental setup was explained, and wall pressure plots, as well as static and pitot pressure measurements along the height and width of the intake exit were discussed for three different configurations. In addition, the intake behavior under pressure fluctuations coming from the combustion chamber was investigated by imposing a certain back pressure with a throttle. Furthermore, the numerical setup was explained, and the wind tunnel, as well as flight conditions which we used, were presented. Finally, an analytical post-analysis was performed, in which we modeled the property change in the combustion chamber with a *Rayleigh flow* and *flow with friction and area change* analysis. The main findings were:

1. When imposing an artificial back pressure on the intake, the maximum pressure ratio before intake unstart was 120 and 80 for the Mach 7 and 6 cases, respectively; the ratio of maximum pressure ratio to operating pressure ratio was constant at ≈ 4, independent from the configuration.

2. With DLR-TAU we were able to accurately simulate the intake flow field and the numerical simulations matched the experimental results well; deviations were present in the internal portion of the intake only, and can be explained by shifted shock positions.

Table 3: Stream thrust averaged exit conditions, extracted from CFD for flight conditions, along with intake performance parameter.

	$M = 7$, v-lip	$M = 7$, s-lip	$M = 6$, v-lip
M_{cc}	3.1180	3.1265	2.7728
p_{cc} [Pa]	43811	42579	47344
T_{cc} [K]	798.99	796.11	703.09
Π_{st}	28.6683	27.8621	22.762
Π_{tot}	0.30333	0.29852	0.37532
η_{KE}	0.95856	0.95790	0.95512
$h_{\mathrm{t,cc}}/h_{\mathrm{t},\infty}$	0.96812	0.96811	0.97573
$\dot{m}_{\mathrm{cc}}/\dot{m}_{\infty}$	0.88810	0.86704	0.77628
$\varphi_{\max}$	0.47	0.47	0.30
F_{sp} [N/(kg/s)]	334.00	332.34	253.81
I_{sp} [s]	2467.3	2455.1	2937.4
η_{oa}	0.42476	0.42265	0.43151
φ	0.30	0.30	0.30
F_{sp} [N/(kg/s)]	124.75	124.47	253.81
I_{sp} [s]	1443.7	1440.5	2937.4
η_{oa}	0.24854	0.24800	0.43151

3. The analytical post-analysis was a good mean to investigate and directly compare similar intake configurations; the v-shaped and straight lip configuration had a maximum specific impulse of 2467 s and 2455 s for Mach 7. Nevertheless, one should be aware of the simplicity of the assumptions within.

4. In-stream measurements at the intake exit also showed good agreement with the numerical simulations; however the overall deviations and measurement uncertainties were higher. Generally the intake flow field was three-dimensional and the variation was larger across the intake height.

Acknowledgments

The present work was funded during the Research Training Group 1095/2 (2005-2014). We would like to thank the German Research Foundation (DFG) for the support during that period. Furthermore we would like to thank Michael Kosbow and Marco Schmors for the operation of the wind tunnel and the technical support.

References

[1]Riehmer, J. C., *Auslegung eines Scramjet-Flugexperiments und aerothermodynamische Analyse*, submitted, RWTH Aachen, 2015.

[2]Billig, F. S. and Wie, D. M. V., "Efficiency Parameters for Inlets Operating at Hypersonic Speeds," Tech. rep., 1987.

[3]Heiser, W. H. and Pratt, D. T., *Hypersonic Airbreathing Propulsion*, AIAA Education Series, 1994.

[4]Smart, M. K., "How Much Compression Should a Scramjet Inlet Do ?" *AIAA Journal*, Vol. 50, No. 3, 2012, pp. 610–619.

[5]Flock, A. K. and Gülhan, A., "Experimental Investigation of the Starting Behavior of a Three-Dimensional Scramjet Intake," *AIAA Journal*, Feb. 2015, pp. 1–8.

[6]Hohn, O. M. and Gülhan, A., "Analysis of a Three-Dimensional , High Pressure Ratio Scramjet Inlet with Variable Internal Contraction," *18th AIAA/3AF International Space Planes and Hypersonics Systems and Technologies Conference*, No. September, 2012.

[7]Riehmer, J. C. and Gülhan, A., "Simulation of combustion by cold air injection in a generic scramjet model in the H2K blow down facility," *5th European Conference for Aeronautics and Space Sciences*, 2013.

[8]Pinckney, S. Z., "An Improved Static Probe Design," *AIAA Journal*, Vol. 12, No. 4, 1973, pp. 562–564.

[9]Tropea, C., Yarin, A. L., and Foss, J. F., *Handbook of Experimental Fluid Mechanics*, Springer, Berlin, Heidelberg, 2007.

[10]Niezgoda, F.-J., "Der Hyperschallwindkanal H2K des DLR in Köln-Porz," Tech. rep., Deutsches Zentrum für Luft- und Raumfahrt, 2001.

[11]Mack, A. and Hannemann, V., "Validation of the Unstructured DLR-TAU-Code for Hypersonic Flows," *32nd AIAA Fluid Dynamics Conference and Exhibit*, No. June, 2002.

[12]Menter, F. R., Kuntz, M., and Langtry, R., "Ten Years of Industrial Experience with the SST Turbulence Model," *Heat and Mass Transfer*, Vol. 4, 2003.

[13]Zucrow, M. J. and Hoffman, J. D., *Gas Dynamics Volume I*, John Wiley & Sons, 1976.

[14]Oosthuizen, P. H. and Carscallen, W. E., *Compressible Fluid Flow*, McGraw Hill, 1997.

[15]Anderson, J. D. J., *Fundamentals of Aerodynamics Fourth Edition*, McGraw Hill, 2007.